

# Global Decay Chain Vertex Fitting at $B$ -Factories

J.-F. Krohn<sup>★a</sup>, P. Urquijo<sup>a</sup>, F. Abudinén<sup>d</sup>, S. Cunliffe<sup>b</sup>, T. Ferber<sup>b</sup>, M. Gelb<sup>c</sup>,  
 J. Gemmler<sup>c</sup>, P. Goldenzweig<sup>c</sup>, T. Keck<sup>c</sup>, I. Komarov<sup>b</sup>, T. Kuhr<sup>e</sup>, L. Ligioli<sup>d</sup>,  
 M. Lubej<sup>f</sup>, F. Meier<sup>g</sup>, F. Metzner<sup>c</sup>, C. Pulvermacher<sup>c</sup>, M. Ritter<sup>e</sup>,  
 U. Tamponi<sup>h</sup>, F. Tenchini<sup>b</sup>, A. Zupanc<sup>f</sup>

*Belle II analysis software group*

<sup>a</sup>*University of Melbourne, Melbourne, Australia*

<sup>b</sup>*Deutsches Elektronen-Synchrotron, Hamburg, Germany*

<sup>c</sup>*Karlsruhe Institute of Technology, Karlsruhe, Germany*

<sup>d</sup>*Max-Planck-Institut für Physik, Munich, Germany*

<sup>e</sup>*Ludwig Maximilians Universität, Munich, Germany*

<sup>f</sup>*Jožef Stefan Institute, Ljubljana, Slovenia*

<sup>g</sup>*University of Sydney, Sydney, Australia*

<sup>h</sup>*INFN - Sezione di Torino, Torino, Italy*

---

## Abstract

We present a particle vertex fitting method designed for  $B$  factories. The presented method uses a Kalman Filter to solve a least squares estimate to globally fit decay chains, as opposed to traditional methods that fit each vertex at a time. It allows for the extraction of particle momenta, energies, vertex positions and flight lengths, as well as the uncertainty estimates of these quantities. Furthermore, it allows for the precise extraction of vertex parameters in complex decay chains containing neutral final state particles, such as  $\gamma$  or  $K_L^0$ , which cannot properly be tracked due to limited spatial resolution of longitudinally segmented single-layer crystal calorimeters like the Belle II ECL. The presented technique can be used to suppress combinatorial background and improve resolutions on measured parameters. We present studies using Monte Carlo simulations of collisions in the Belle II experiment, where modes with neutrals are crucial to the physics analysis program.

---

## 1. Introduction

2 Particle vertex fitting techniques are widely used in particle and nuclear  
 3 physics. Beyond the suppression of background, applications range from the  
 4 improvement of particle momentum resolution (under the assumption they origi-  
 5 nate from some vertex point), to the determination of the presence of interme-  
 6 diate particles and the precision determination of decay vertex positions. One

---

<sup>★</sup>Corresponding author.

Email: jkrohn@student.unimelb.edu.au

can, for example, combine the measurements of two charged pion tracks originating from the decay of a  $K_S^0$  to extract the decay vertex position, flight length and four-vector and their uncertainties. By performing a kinematic fit, one obtains an improvement of the pion track momenta and can use the  $\chi^2$  probability of the fit result to suppress background.

In order to construct more complex decay topologies, one usually combines cascades of these fits starting with long lived stable particles such as electrons, muons, pions and photons, forming intermediate resonances and finally the full decay of interest. For example, in the decay  $B^0 \rightarrow J/\Psi K_S^0$ , where  $J/\Psi \rightarrow \mu^+ \mu^-$  and  $K_S^0 \rightarrow \pi^+ \pi^-$ , one would first fit the  $J/\Psi$  and  $K_S^0$  candidates and then use these to construct the  $B^0$  candidates, as depicted in Fig. 1a and Fig. 1b. However, this only works well if the final state particles are charged and leave traces in the tracking detectors. Neutral particles can not be tracked; they are only measured by their energy deposition in the calorimeter. Single layer crystal calorimeters do not offer directional information on where the particle associated to an energy deposition originated from. This means that the decay vertex can not be extracted from the fit. In order to obtain the momentum vector, it has to be assumed that the particle originates from the primary interaction point and travels directly into the cluster's center of gravity. This can introduce a large bias on the momentum components. Consider, for example, the decay  $B^0 \rightarrow J/\Psi K_S^0$ , where the kaon instead decays to neutral final states,  $K_S^0 \rightarrow \pi^0 \pi^0$ , and the pions decay,  $\pi^0 \rightarrow \gamma \gamma$ , as displayed in Fig. 2. Weakly decaying intermediate particles such as  $K_S^0$  have relatively long flight lengths, up to 15 cm for  $K_S^0$  at Belle II. Thus for a neutral particle in such a particle decay chain, the assumption that it originates from the primary  $e^+e^-$  collision is not sufficient.

The method we present in this paper overcomes these issues by globally fitting the entire decay tree in a single fit, taking into account all intermediate particles, extracting all involved particle's four-momenta, vertex positions, flight lengths and their covariance matrices, using a Kalman Filter as described in Ref. [1]. We use the software environment of Belle II and rely on the C++ template library EIGEN [2] for matrix operations, which provides a fast execution time for the fit algorithm. We furthermore present physics applications of the fitter with Belle II Monte Carlo samples.

### 1.1. The Belle II Experiment

The algorithm described in this paper was developed for the analysis software framework of Belle II. The Belle II experiment takes place at the asymmetric  $e^+e^-$  collider, SuperKEKB. SuperKEKB provides a beam energy slightly above the mass of the  $\Upsilon(4S)$  resonance ( $10.58 \text{ GeV}/c^2$ ) at an instantaneous luminosity of  $8 \cdot 10^{35} \text{ cm}^{-2}\text{s}^{-1}$ . The  $\Upsilon(4S)$  resonance decays into pairs of  $B$ -mesons just above production threshold, hence this type of experiment is referred to as a  $B$ -factory. The asymmetric beam energy gives the  $B$ -meson a relativistic boost along a direction close to the detector's axis of symmetry, increasing its flight length in the lab frame, which makes it easier to study the time evolution of  $B$  decays - a key observable in the study of CP symmetry violation.

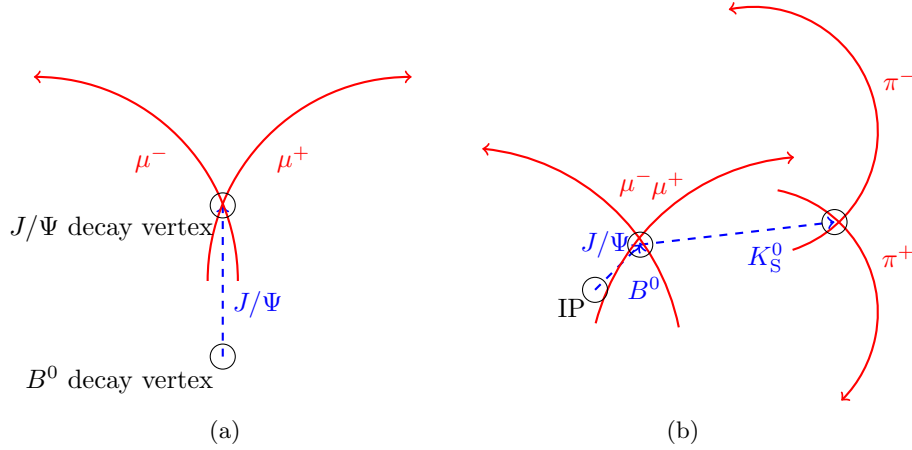


Figure 1: a) Depiction of a  $J/\Psi \rightarrow \mu^+\mu^-$  decay. The red lines show the track helix approximations obtained from the tracking detectors, the blue dashed lines show the decaying particle momentum vectors found by the fit. Since the decay length of the  $J/\Psi$  is too short to be seen in the detector, its decay vertex is taken to be the one of the  $B^0$ . b) Depiction of a  $B^0 \rightarrow J/\Psi(\rightarrow \mu^+\mu^-)K_S^0(\rightarrow \pi^+\pi^-)$  decay. Measured track helices do not necessarily overlap in three dimensions. The depicted length ratios are not to scale.

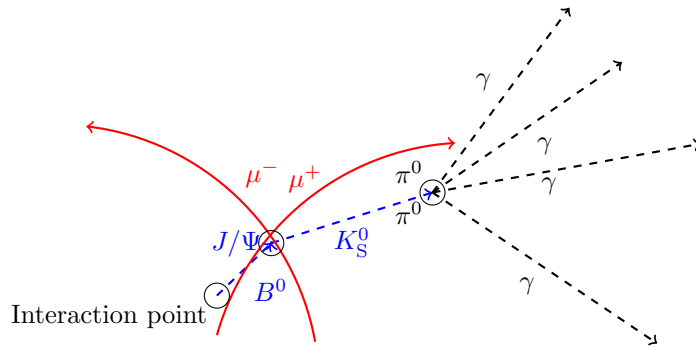


Figure 2: Depiction of a the decay  $B^0 \rightarrow K_S^0 J/\Psi$ . The red lines show the track helix approximations obtained by the tracking detectors, the blue dashed lines show the composite particle momentum vectors found by the fit. The dashed black lines depict the photon momenta found by the fit. Note that these can only be extrapolated by the fit as the directional information of the calorimeter is not sufficient. The initial guess is that they point from the interaction point towards the calorimeter cluster. The decay lengths of the  $J/\Psi$  and  $\pi^0$  are too short to be seen in the detector therefore the vertex positions are taken from the particle above them in the hierarchy.

The Belle II detector has a cylindrical structure designed to study the decays of  $B$ - and  $D$ -mesons,  $\tau$ -leptons and other processes produced in  $e^+e^-$  collisions. Six layers of silicon vertex detectors (2 layers of silicon pixels (PXD), and 4 layers of double sided silicon detectors (SVD)) are located in the central volume of the detector, designed to accurately track the flight paths of charged particles. The following layers are, a central drift chamber (CDC) used to measure track trajectories within a solenoid magnetic field, Cherenkov light based particle identification devices surrounding the CDC in the barrel (TOP) and forward regions (ARICH), followed by the CsI(Tl) electromagnetic calorimeter (ECL). The outermost layers are composed of, a magnet solenoid, a  $K_L^0$  and muon detector system (KLM), which is also used as the flux return yoke of the magnet. The magnetic field is aligned along the detector's axis of symmetry. For a more detailed description of the detector see Ref. [3].

Fig. 3 and Fig. 4 show an event display depicting simulated particles traversing the Belle II detector. In the decay  $\Upsilon(4S) \rightarrow \bar{B}^0 B^0$ , one meson decays as  $\bar{B}^0 \rightarrow D\omega\pi\pi$ , and the other as  $B^0 \rightarrow K_S J/\Psi$ , with  $J/\Psi \rightarrow \mu^+\mu^-$  and  $K_S^0 \rightarrow \pi^0\pi^0$  with  $\pi^0 \rightarrow \gamma\gamma$ . Fig. 3, depicts the full detector geometry and Fig. 4 shows a close-up of the inner vertex detectors. In this example we show that the decay vertex of the  $K_S^0$  can be very displaced.

## 2. Extended Kalman Filter

Vertex fitting is a least squares minimization problem. The best least squares estimator (LSE) is the solution to this problem. The computational challenge in finding a LSE lies in matrix inversions, which naively scale as  $\mathcal{O}(n^3)$ , where  $n$  is the dimension of the matrix. In a naive approach, this is equal to the number of parameters extracted in the fit. A Kalman Filter is an iterative approach to find the LSE by defining a series of constraints (knowledge of parameters from measurements and symmetries) on a hypothesis (a set of particle parameters in this case). The hypothesis has different states during the stages of the filtering process. The filtering process is an iterative algorithm applying the constraints sequentially and updating the state with respect to the constraints. The sequence is repeated until convergence is reached or divergence is observed. In the case of convergence, the last state describes the best hypothesis for the parameters that can be found. We use an Extended Kalman Filter in the gain matrix formulation [4, 5, 1] in our algorithm. The state vector  $\mathbf{x}$  holds the particle parameters to be optimized by the fit. The parameters depend on the type of particle. The most general parametrization takes the form

$$\mathbf{x} = \{x_1, y_1, z_1, \theta_1, p_{x1}, p_{y1}, p_{z1}, E_1, \dots, x_n, y_n, z_n, \theta_n, p_{xn}, p_{yn}, p_{zn}, E_n\}, \quad (2)$$

where vertex coordinates of the  $i$ -th particle are denoted as  $\{x_i, y_i, z_i\}$ , its decay length is denoted as  $\theta_i$  and the four momentum is  $\{p_{x,i}, p_{y,i}, p_{z,i}, E_i\}$ , and  $n$  is the number of particles in the fitted topology. This implies that  $n \approx 8 \times$  number of particles. The problem is split into  $k$  constraints given by measurements and other knowledge of parameters (see Sec. 3 for the definitions

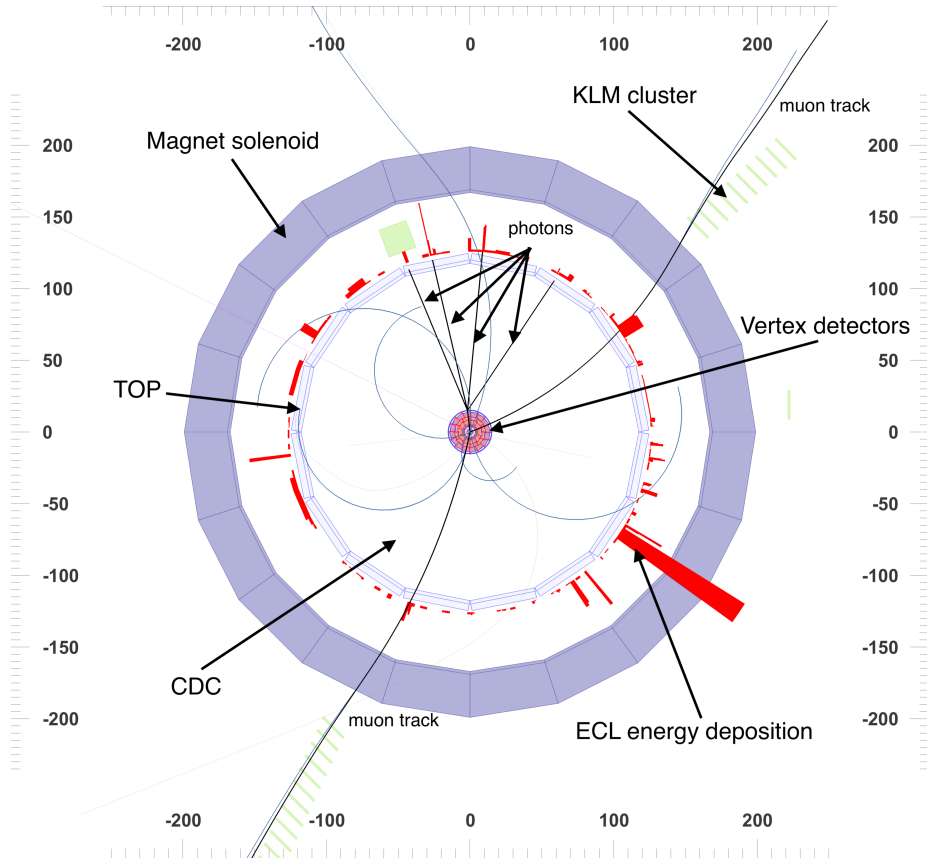


Figure 3: Event display projected onto the  $x - y$  plane depicting the process of  $\bar{e}^+e^- \rightarrow \Upsilon(4S) \rightarrow \bar{B}^0 B^0$ , with  $\bar{B}^0 \rightarrow D\omega\pi\pi$  and  $B^0 \rightarrow K_S J/\Psi$ , where  $J/\Psi \rightarrow \mu^+\mu^-$  and  $K_S^0 \rightarrow \pi^0\pi^0$  with  $\pi^0 \rightarrow \gamma\gamma$ . All particles of the signal  $B^0$  decay are indicated by black lines. The rest of the event correspond to the decay of the  $\bar{B}^0$ . All distances are measured in centimetres. For a close-up of the vertex detector see Fig. 4.

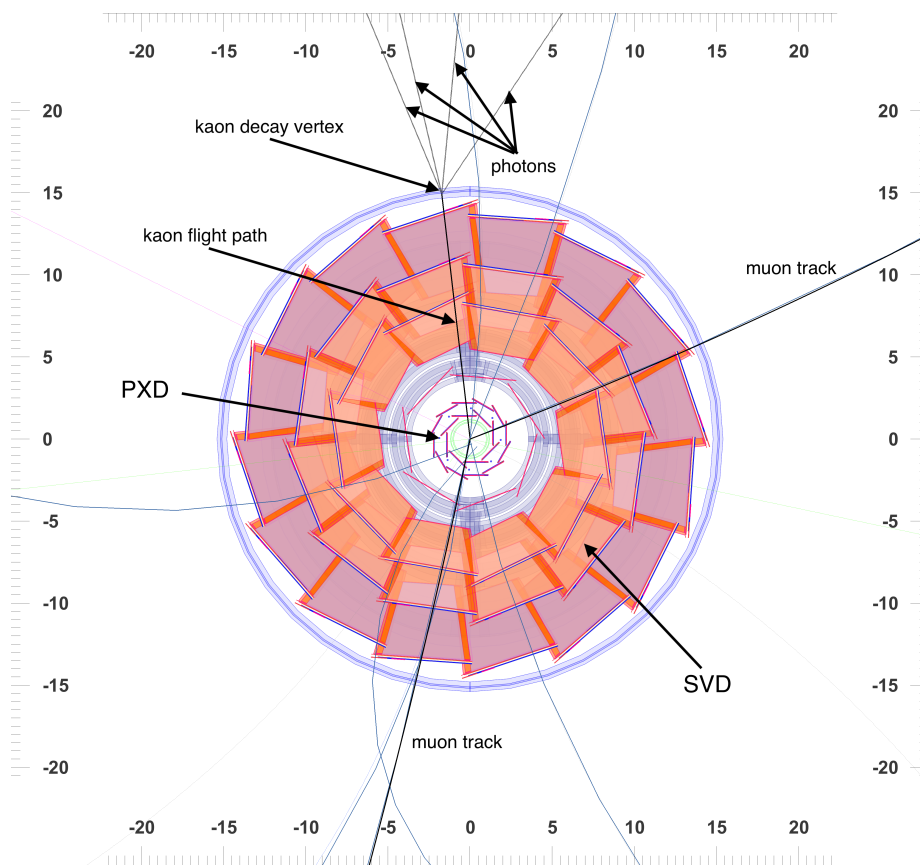


Figure 4: Close-up of Fig. 3. In this event, the  $K_S^0$  travels until the edge of the vertex detectors before decaying.

of the measurement  $\mathbf{m}$  and hypothesis  $\mathbf{h}$  for each of the different constraints).  
 94 The minimized  $\chi^2$  can be expressed as a weighted sum of  $k$  sets of equations,  
 which are the constraints. For a given iteration,  $\alpha$ , of the Kalman Filter, one  
 96 can write

$$\chi_\alpha^2 = (\mathbf{m}_1 - \mathbf{h}_1(\mathbf{x}_0^\alpha))^T \mathbf{V}_1^{-1} (\mathbf{m}_1 - \mathbf{h}_1(\mathbf{x}_0^\alpha)) + \dots \quad (3)$$

$$+ (\mathbf{m}_k - \mathbf{h}_k(\mathbf{x}_{k-1}^\alpha))^T \mathbf{V}_k^{-1} (\mathbf{m}_k - \mathbf{h}_k(\mathbf{x}_{k-1}^\alpha)),$$

98 using the measurement covariance matrix  $\mathbf{V}_k^{-1}$  transported to the  $\mathbf{m} - \mathbf{h}$   
 system as a weight, such that the hypothesis of each constraint  $k$  depends on the  
 100 outcome of the previous constraint.

Minimizing Eq. 3 yields a rule to find a new state  $\mathbf{x}_k^\alpha$  for the current iteration  
 102 and constraint, that is

$$\mathbf{x}_k^\alpha = \mathbf{x}_{k-1}^\alpha - \mathbf{K}_k^\alpha \mathbf{r}_k^\alpha, \quad (4)$$

104 where  $\mathbf{K}$  is a gain matrix, which will be defined below. However, we first define  
 the residual  $r$  as the distance between measurement and hypothesis

$$\mathbf{r}_k^\alpha = \mathbf{m}_k - \mathbf{h}_k(\mathbf{x}^\alpha). \quad (5)$$

The hypothesis  $\mathbf{h}_k(\mathbf{x}^\alpha)$  can be linearised around a reference state of the previous  
 108 iteration  $\mathbf{x}^{\alpha-1}$  using the Jacobian

$$\mathbf{H}_k^{\alpha-1} = \frac{\partial \mathbf{h}_k(\mathbf{x}^{\alpha-1})}{\partial \mathbf{x}^{\alpha-1}}, \quad (6)$$

110 such that

$$\mathbf{h}_k(\mathbf{x}^\alpha) = \mathbf{h}_k(\mathbf{x}^{\alpha-1}) - \mathbf{H}_k^{\alpha-1} \cdot (\mathbf{x}^\alpha - \mathbf{x}^{\alpha-1}). \quad (7)$$

112 Eq. 5 thus becomes

$$\mathbf{r}_k^\alpha = \mathbf{m}_k - \mathbf{h}_k(\mathbf{x}^{\alpha-1}) + \mathbf{H}_k^{\alpha-1} \cdot (\mathbf{x}^\alpha - \mathbf{x}^{\alpha-1}). \quad (8)$$

114 The gain matrix is calculated for every constraint in every iteration and is  
 defined as

$$\mathbf{K}_k = \mathbf{C}_{k-1} \mathbf{H}_k^T \mathbf{R}_k^{-1}. \quad (9)$$

The only matrix to be inverted is of the dimension of the constraint and not the  
 118 dimension of the statespace. The current state's covariance matrix is obtained  
 via propagation of uncertainties

$$\begin{aligned} \mathbf{C}_k &= (1 - \mathbf{K}_k \mathbf{H}_k) \mathbf{C}_{k-1} (1 - \mathbf{K}_k \mathbf{H}_k)^T \\ &= \mathbf{C}_{k-1} - \mathbf{C}_{k-1} \mathbf{H}_k \mathbf{R}_k^{-1} \mathbf{H}_k \mathbf{C}_{k-1}^T \\ &= \mathbf{C}_{k-1} - \mathbf{C}_{k-1} \mathbf{H}_k^T \mathbf{K}_k^T. \end{aligned} \quad (10)$$

The covariance matrix of the residual system can be found to be

$$\mathbf{R}_k = \mathbf{V}_k + \mathbf{H}_k \mathbf{C}_{k-1} \mathbf{H}_k^T. \quad (11)$$

For constraints where no measurement is available, for example the mass con-  
 124 straint, we set  $\mathbf{V}_k = 0$ .

Linearising the hypothesis around a reference state, see Eq. 7, makes the fits  
 126 more stable than a normal Kalman Filter and reduces the overall number of  
 signal candidates for which the fit diverges. In this formulation of the LSE  
 128 problem, the update of the covariance matrix, Eq. 10, is the computational bot-  
 tleneck, as it is a dense  $m \times m$  matrix with the dimension of the state vector  $m$   
 130 and must be calculated and filled  $k$  times for each iteration.

### 3. Parametrising and constraining the decay chain

To parametrise the decay chain, we use a set of parameters that describe the  
 132 properties of the particles. We perform a number of reductions on these prop-  
 134 erties to reduce the dimensionality of the problem. For final state particles, we  
 only save the momenta, as they do not have decay vertices. For their production  
 136 vertices we use the decay vertices of their respective composite particles, later  
 referred to as “mothers”. The energy of each each final state particle is cal-  
 138 culated using the momenta and it’s nominal mass hypotheses, taking the mass  
 values provided by the particle data group (PDG) [6]. Intermediate particles  
 140 are classified in two categories: particles that decay dominantly via the strong  
 force and via the weak force. Strongly decaying particles with a lifetime of less  
 142 than  $10^{-14}$  s, which corresponds to boosted flight lengths of the order of less  
 than  $1 \mu\text{m}$ , are treated as if they instantly decay (the detector has a vertex  
 144 position resolution in the x-y plane for charged particles of  $20 - 30 \mu\text{m}$ ). The  
 hypothesised quantities are their energy and momenta, while the production  
 146 and decay vertices coincide and are taken from their mother particle’s decay  
 vertex. For weakly decaying particles, we additionally measure a decay vertex  
 148 and a flight length, defined as the distance between the production and decay  
 vertices in three dimensions.

#### 3.1. Parametrising the constraints

Constraints are defined by Eq. 7. The resulting Jacobians take the form  
 152 of  $m \times n$  matrices where  $m$  is the dimension of the state vector and  $n$  is the  
 dimension of the respective constraint. Thus, only few of its elements are non-  
 154 zero. For example, for a three dimensional point constraint  $k$ , the hypothesis  
 of particle number  $j$  with  $\mathbf{h}_j = \{x_j, y_j, z_j\}$  and  $\mathbf{x}$  as in Eq. 2, only the  $j$ -th  
 156 diagonal block is non-zero

$$\frac{\partial \mathbf{h}}{\partial \mathbf{x}} = \mathbf{H} = \begin{pmatrix} 0 & \mathbb{1}_3 & 0 \end{pmatrix}. \quad (12)$$

158 The blocks filled with zero correspond to the parameters of particle  $\mathbf{x}_i \neq \mathbf{x}_j$ .  
 We will omit the columns filled with zeros throughout this section, for brevity.  
 160 In the following we list the definitions of constraints that have been implemented  
 in the Belle II software, based on the specific geometry of Belle II.



162 *3.1.1. Reconstructed track*

164 A track can be parametrised with a five parameter helix. In Belle II it was  
 165 chosen to use a perigee-parametrised helix, such that the helix is defined at the  
 166 perigee, the point of closest approach of the helix to the origin of the coordinate  
 167 system. The corresponding transformations to transport a helix to that point  
 168 are discussed in Ref. [7]. A description of the parameters can be found in Table 1,  
 and a depiction of the helix is in Fig. 5. We parametrise tracks such that we  
 can express the model's dependence on Cartesian parameters as

$$170 \quad \mathbf{h}_{\text{track}}(\mathbf{x}) = \begin{pmatrix} d_0 \\ \phi_0 \\ \omega \\ z_0 \\ \tan \lambda \end{pmatrix} = \begin{pmatrix} A(1+U)^{-1} \\ \text{atan2}(p_y, p_x) - \text{atan2}(\omega \cdot \Delta_{\parallel}, 1 + \omega \cdot \Delta_{\perp}) \\ a \cdot q/p_t \\ z + l \cdot \tan \lambda \\ p_z/p_t \end{pmatrix}. \quad (13)$$

Where  $\text{atan2}$  refers to the phi domain corrected inverse tangent function. We  
 172 use the same parametrisation for the hypothesis and the measurement. We label  
 the measurement quantities with the index  $m$ . The residuals of iteration  $\alpha$  then  
 174 become

$$\mathbf{r}_{\text{track}}^{\alpha}(\mathbf{x}) = \begin{pmatrix} d_{0,m} - d_0 \\ \phi_{0,m} - \phi_0 \\ \omega_m - \omega \\ z_{0,m} - z_0 \\ \tan \lambda_m - \tan \lambda \end{pmatrix} + \mathbf{H}^{\alpha-1} \cdot (\mathbf{x}^{\alpha} - \mathbf{x}^{\alpha-1}). \quad (14)$$

176 We define the Jacobian block  $\mathbf{A} := \partial \mathbf{h} / \partial \mathbf{x}$  as the derivatives with respect to the  
 vertex position, and  $\mathbf{B} := \partial \mathbf{h} / \partial \mathbf{p}$  as the derivatives with respect to momentum.  
 178 The positions of these blocks in the Jacobian depend on the topology fitted  
 and the particle represented by the track. We choose to order the state vector  
 180 hierarchically. This means that the decay vertex parameters come before its  
 momentum, followed by the daughter particle's parameters. The full Jacobian  
 182  $\mathbf{H}$  then takes the following form

$$\mathbf{H} = \begin{pmatrix} \dots & \dots & \dots \\ \dots & \dots & \dots \\ \dots & \mathbf{A} & \dots & \mathbf{B} & \dots \\ \dots & \dots & \dots & \dots & \dots \\ \dots & \dots & \dots & \dots & \dots \end{pmatrix}. \quad (15)$$

184 For the non-zero elements of the Jacobian blocks, denoted by  $\partial d_0 / \partial x = \mathbf{A}_{d_0,x}$ ,  
 we derive the spatial components as

$$186 \quad \begin{aligned} \mathbf{A}_{d_0,x} &= \frac{p_{y0}}{p_{t0}}, & \mathbf{A}_{d_0,y} &= -\frac{p_{x0}}{p_{t0}}, \\ \mathbf{A}_{\phi_0,x} &= \frac{a \cdot q \cdot p_{x0}}{p_{t0}^2}, & \mathbf{A}_{\phi_0,y} &= \frac{a \cdot q \cdot p_{y0}}{p_{t0}^2}, \\ \mathbf{A}_{z_0,x} &= -\frac{p_x \cdot p_{x0}}{p_{t0}^2}, & \mathbf{A}_{z_0,y} &= -\frac{p_x \cdot p_{y0}}{p_{t0}^2}, & \mathbf{A}_{z_0,z} &= 1, \end{aligned} \quad (16)$$

Table 1: Definitions of the Belle II helix parametrisation and their dependencies.

$d_0$	The distance of closest approach to the $z$ axis (POCA) signed with the $z$ component of the angular momentum w.r.t. to the origin.
$\phi_0$	Azimuthal angle of the momentum at the POCA.
$\omega$	Scaled inverse of the track momentum.
$z_0$	The pivotal point is the perigee that is the POCA.
$\tan \lambda$	The angle of the momentum at the POCA with respect to the $x - y$ plane.
$\phi = \text{atan2}(p_y, p_x)$	Angle of the $x - y$ plane to the helix.
$\Delta_{\parallel} = -x \cdot \cos \phi - y \cdot \sin \phi$ $\Delta_{\perp} = -y \cdot \cos \phi + x \cdot \sin \phi$ $A = 2 \cdot \Delta_{\perp} + \omega \cdot (\Delta_{\perp}^2 + \Delta_{\parallel}^2)$ $U = \sqrt{1 + \omega \cdot A}$ $\lambda$	Quantities used to transport the coordinate system, such that $\{x, y, z\}$ points to the perigee.
$l = \text{atan2}(\omega \cdot \Delta_{\parallel}, 1 + \omega \cdot \Delta_{\perp})$	Angle between the $x - y$ plane and the helix.
$p_x, p_y, p_z$	Arc length from the perigee to a point.
$q$	Momenta along the $x, y, z$ axes.
$B_z$	Charge of the particle.
$a = B_z/c$	Magnetic field strength in $z$ -direction.
$p_t = \sqrt{p_x^2 + p_y^2}$	Magnetic field strength in the $z$ direction divided by the speed of light.
$p_{t0} = \sqrt{p_{x0}^2 + p_{y0}^2}$	Transverse momentum.
$p_{x0} = p_x - a \cdot q \cdot y$	Pseudo transverse momentum.
$p_{y0} = p_y + a \cdot q \cdot x$	Pseudo momentum along the $x$ direction.
$r^2 = x^2 + y^2$	Pseudo momentum along the $y$ direction.
$\beta = 1 + \frac{p_{t0}}{p_t}$	Radius squared.
	Quantity used for reading convenience.

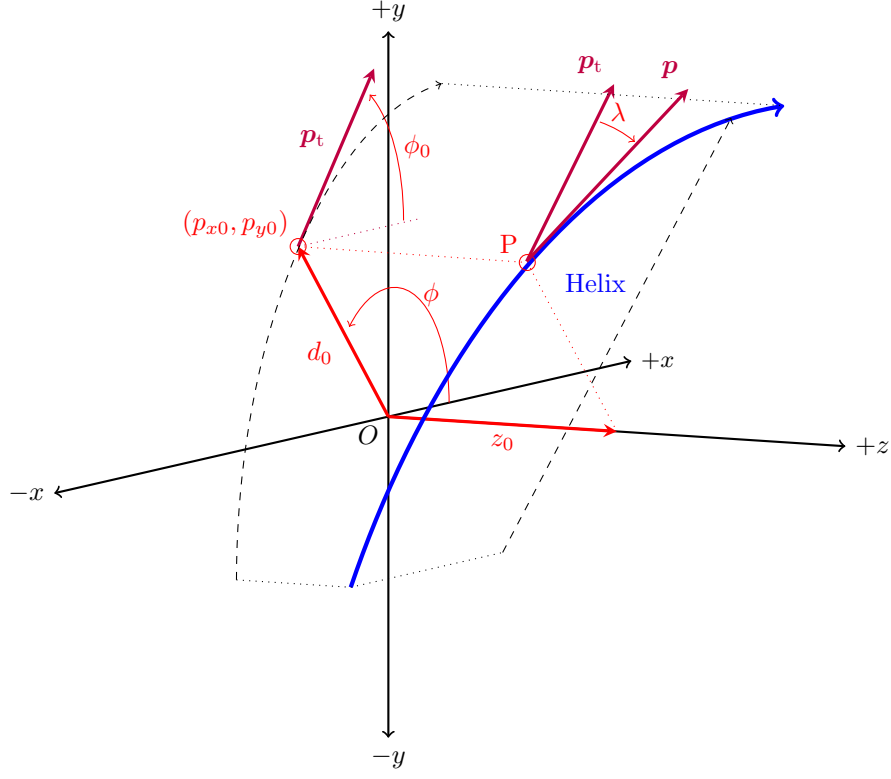


Figure 5: The perigee parametrisation of the track helix, depiction adapted from [8]. A description of the parameters can be found in Tab. 1.

and for the momenta

$$\begin{aligned}
 \mathbf{B}_{d_0, p_x} &= - \frac{y((aq)^2 r + 2aq p_y x + 2p_y^2 \beta)}{p_{t0} p_t^2 \beta^2} \\
 &\quad - \frac{p_x(2p_y x \beta + aq(y^2(-2 + \beta) + x^2 \beta))}{p_{t0} p_t^2 \beta^2}, \\
 \mathbf{B}_{d_0, p_y} &= \frac{2p_x^2 x \beta + 2p_x y(p_y - aqx + p_y p_{t0}/p_t)}{p_{t0} p_t^2 \beta^2} \\
 &\quad + \frac{aq(aqr x - p_y(x^2(-2 + \beta) + y^2 \beta))}{p_{t0} p_t^2 \beta^2},
 \end{aligned} \tag{17}$$

188

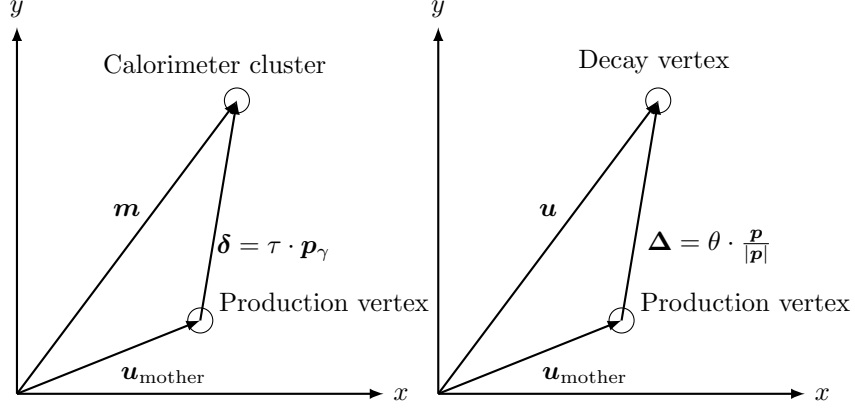


Figure 6: (a) The photon constraint, Eq. 21, reduced to two dimensions for simplicity. The vector  $\delta$  is defined as pointing from the photon's production vertex to the measured calorimeter cluster, indicated with the photons mother's coordinate vector  $\mathbf{u}$  and measurement vector  $\mathbf{m}$ . (b) Geometric constraint, Eq. 31. The vector  $\Delta$  is defined pointing from the particles decay and production vertex, indicated with the particle's and its mother's coordinate vector  $\mathbf{u}$ .

and

$$\begin{aligned}
\mathbf{B}_{\omega,p_x} &= -\frac{aqp_x}{p_t^3}, \quad \mathbf{B}_{\omega,p_y} = -\frac{aqp_y}{p_t^3}, \\
\mathbf{B}_{z_0,p_x} &= \frac{p_z(p_x^2x - p_y(aqr + p_yx) + 2p_xp_yy)}{p_{t0}^2p_t^2}, \\
\mathbf{B}_{z_0,p_y} &= \frac{p_z(p_x(aqr + 2p_yx) - p_x^2y + p_y^2y)}{p_{t0}^2p_t^2}, \\
\mathbf{B}_{z_0,p_z} &= (aq)^{-1} \text{atan2}(aq(p_yy - p_xx), p_x^2 + p_y p_{y0} - aqp_xy), \\
\mathbf{B}_{\tan \lambda,p_x} &= -\frac{p_z p_x}{p_t^3}, \quad \mathbf{B}_{\tan \lambda,p_y} = -\frac{p_z p_y}{p_t^3}, \quad \mathbf{B}_{\tan \lambda,p_z} = p_t^{-1}.
\end{aligned} \tag{18}$$

### 3.1.2. Reconstructed photon

For photons we measure the position of the calorimeter cluster and its energy and can infer the vertex parameters. The geometry, depicted in Fig. 6, gives

$$0 = \mathbf{u}_{\text{mother}} + \delta - \mathbf{m}, \tag{19}$$

substituting  $\delta = \tau \cdot \mathbf{p}$  and inserting the energy relation, we get

$$\mathbf{h}_{\text{photon}}(\mathbf{x}) = \begin{pmatrix} u_x + \tau \cdot p_x \\ u_y + \tau \cdot p_y \\ u_z + \tau \cdot p_z \\ \sqrt{p_x^2 + p_y^2 + p_z^2} \end{pmatrix} \quad \text{and} \quad \mathbf{m}_{\text{photon}}(\mathbf{x}) = \begin{pmatrix} m_x \\ m_y \\ m_z \\ E_m \end{pmatrix}, \tag{20}$$

where  $\{u_x, u_y, u_z\}$  are the production vertex coordinates,  $\{p_x, p_y, p_z\}$  are the parameters of the momentum vector pointing from the production vertex to the

calorimeter cluster,  $\{m_x, m_y, m_z, E_m\}$  are the position and measured energy of  
 200 the corresponding ECL cluster. The parameter  $\tau$  is the decay time, which can  
 be eliminated when writing down the residual to reduce the dimensionality of  
 202 the equation system and avoid a trivial local minimum of  $\mathbf{r}_\gamma$  at  $\tau = 0$  when  
 taking  $\{u_x, u_y, u_z\} = 0$  as the starting point of the first iteration. Since the  
 204 geometry of the detector is cylindrical, we can not simply eliminate any of the  
 dimensions as this could introduce a pole in the residual equations. Thus, we  
 206 sort the momenta and eliminate the dimension with the highest momentum.  
 Such that we get a 3-dimensional equation system

$$208 \quad \mathbf{r}'_{\text{photon}}(\mathbf{x}) = \begin{pmatrix} (m_i - u_i) - (m_k - u_k) \frac{p_i}{p_k} \\ (m_j - u_j) - (m_k - u_k) \frac{p_j}{p_k} \\ E_m - \sqrt{p_i^2 + p_j^2 + p_k^2} \end{pmatrix} + \mathbf{H}^{\alpha-1} \cdot (\mathbf{x}^\alpha - \mathbf{x}^{\alpha-1}), \quad (21)$$

where the indices  $i, j, k$  indicate the dimensions by order of increasing momen-  
 210 tum  $p_k \geq p_i \geq p_j$ . We define  $\mathbf{A}_{i,u_k} := \partial h'_i / \partial u_k$  and  $\mathbf{B}_{i,p_k} := \partial h'_i / \partial p_k$  with the  
 hypothesis of the reduced system  $r'$ . Thus, the non-zero entries are

$$212 \quad \begin{aligned} \mathbf{A}_{0,u_k} &= \frac{p_i}{p_k}, & \mathbf{A}_{0,u_i} &= -1, \\ \mathbf{A}_{1,u_k} &= \frac{p_j}{p_k}, & \mathbf{A}_{1,u_j} &= -1, \\ \mathbf{B}_{0,p_k} &= p_k^{-2}, & \mathbf{B}_{0,p_i} &= \frac{u_k - m_k}{p_k}, \\ \mathbf{B}_{1,p_k} &= p_k^{-2}, & \mathbf{B}_{1,p_j} &= \frac{u_k - m_k}{p_k}, \\ \mathbf{B}_{2,p_k} &= -\frac{p_k}{|\mathbf{p}|}, & \mathbf{B}_{2,p_i} &= -\frac{p_i}{|\mathbf{p}|}, & \mathbf{B}_{2,p_j} &= -\frac{p_j}{|\mathbf{p}|}. \end{aligned} \quad (22)$$

The full Jacobian then takes the form

$$214 \quad \mathbf{H} = \begin{pmatrix} \dots & & \dots & & \dots \\ \dots & \mathbf{A} & \dots & \mathbf{B} & \dots \\ \dots & & \dots & & \dots \end{pmatrix}. \quad (23)$$

We must transform the covariance matrix of the measurement into the reduced  
 216 system. For that, we use

$$\mathbf{V}' = \mathbf{F} \mathbf{V} \mathbf{F}^T, \quad (24)$$

218 with the transport matrix  $\mathbf{F} = \partial r' / \partial m$ , which depends on the sorting of the  
 momenta such that the non-zero entries are

$$220 \quad \begin{aligned} \mathbf{F}_{0,m_k} &= -\frac{p_i}{p_k}, & \mathbf{F}_{0,m_i} &= 1, \\ \mathbf{F}_{1,m_k} &= -\frac{p_j}{p_k}, & \mathbf{F}_{1,m_j} &= 1, \\ \mathbf{F}_{2,E_k} &= 1. \end{aligned} \quad (25)$$

We do not parametrise this constraint in  $p_t$  in order to keep the derivatives in  
 222 Eq. 22 as computationally simple as possible.

### 3.1.3. Reconstructed $K_L^0$

224 We treat  $K_L^0$  in the same way as photons, except that we use the nominal  
 225 mass provided by the PDG in the energy calculation. The KLM detector is  
 226 used for the cluster position measurement instead of the calorimeter. It can-  
 227 not provide a precise energy measurement. Instead, it extrapolates the energy  
 228 deposited by a particle as  $E = c \cdot n$ , where  $n$  is the number of hit cells in the  
 229 cluster and  $c$  is a constant with the units GeV. This approach makes the energy  
 230 measurement for  $K_L^0$  much less resolved than for photons.

### 3.1.4. Kinematic constraint

232 The kinematic constraint enforces four-momentum conservation, meaning it  
 fits the four-momentum of the mother as the sum of the daughter momenta

$$234 \quad \mathbf{r}^\alpha(\mathbf{x}) = \mathbf{p}_{\text{particle}} - \sum_i \mathbf{p}_{i,\text{daughter}} + \mathbf{H}^{\alpha-1} \cdot (\mathbf{x}^\alpha - \mathbf{x}^{\alpha-1}). \quad (26)$$

The Jacobian for a particle with *two* daughters, which in this example are taken  
 236 to be stable particles, can be defined

$$\mathbf{H} = \begin{pmatrix} \dots & \dots & \dots & \dots & \dots \\ \dots & \mathbf{A} & \dots & \dots & \dots \\ \dots & \dots & \mathbf{B}_1 & \dots & \mathbf{B}_2 & \dots \\ \dots & \dots & \dots & \dots & \dots & \dots \end{pmatrix}, \quad (27)$$

238 with the blocks  $\mathbf{A}, \mathbf{B}$  as

$$\mathbf{A} = \frac{\partial \mathbf{h}}{\partial \mathbf{p}_{\text{particle}}} = \mathbb{1}_4, \quad (28)$$

240 and

$$\mathbf{B}_i = \frac{\partial \mathbf{h}}{\partial \mathbf{p}_{\text{daughter},i}} = -1 \begin{pmatrix} 1 & & & \\ & 1 & & \\ & & 1 & \\ p_{x,i}/E_i & p_{y,i}/E_i & p_{z,i}/E_i & 0 \end{pmatrix}, \quad (29)$$

242 Note that the energy row of  $\mathbf{B}_i$  depends on how the particle is parametrised,  
 composite particles, for example, are parametrised with an energy variable in  
 244 the state vector, resulting in  $\mathbf{B} = -\mathbb{1}_4$ , while for stable particles Eq. 29 is used.

### 3.1.5. Geometric constraint

246 The geometric constraint fits the decay length parameter  $\theta$  for composite  
 particles, see Fig. 6. Accounting for the geometry we have

$$248 \quad 0 = \mathbf{u}_{\text{mother}} + \mathbf{\Delta} - \mathbf{u}. \quad (30)$$

Instead of directly extracting a flight vector  $\mathbf{\Delta}$ , we use the unit vector of the  
 250 momentum as it is well constrained by the previously filtered kinematic con-  
 straints, substituting  $\mathbf{\Delta} = \theta \cdot \mathbf{p}/|\mathbf{p}|$ , allows for a more accurate estimation of  $\theta$ .  
 252 Thus we define the residual as

$$\mathbf{r}^\alpha(\mathbf{x}) = \mathbf{u}_{\text{mother}} + \theta \cdot \frac{\mathbf{p}}{|\mathbf{p}|} - \mathbf{u} + \mathbf{H}^{\alpha-1} \cdot (\mathbf{x}^\alpha - \mathbf{x}^{\alpha-1}). \quad (31)$$

254 using

$$\mathbf{A} = \frac{\partial \mathbf{h}}{\partial \mathbf{u}_{\text{mother}}} = \mathbb{1}_3, \quad \mathbf{B} = \frac{\partial \mathbf{h}}{\partial \mathbf{u}} = -\mathbb{1}_3, \quad \mathbf{C} = \frac{\partial \mathbf{h}}{\partial \theta} = \frac{1}{|\mathbf{p}|} \begin{pmatrix} p_x \\ p_y \\ p_z \end{pmatrix}, \quad (32)$$

256 and

$$\mathbf{D} = \frac{\partial \mathbf{h}}{\partial \mathbf{p}} = \frac{\theta}{|\mathbf{p}|^3} \begin{pmatrix} (p_y^2 + p_z^2) & -p_x p_y & -p_x p_z \\ -p_y p_x & (p_x^2 + p_z^2) & -p_y p_z \\ -p_z p_x & -p_z p_y & (p_x^2 + p_y^2) \end{pmatrix}, \quad (33)$$

258 such that

$$\mathbf{H} = \begin{pmatrix} \dots & \mathbf{A} & \dots & \mathbf{B} & \dots & \mathbf{C} & \dots & \mathbf{D} & \dots \\ \dots & & \dots & & \dots & & \dots & & \dots \\ \dots & & \dots & & \dots & & \dots & & \dots \end{pmatrix}. \quad (34)$$

### 260 3.1.6. Mass constraint

262 The mass constraint requires a particle four-vector to be consistent with its nominal mass. We treat the particle as a measurement with infinite precision and use the mass value provided by PDG such that

$$264 \quad r^\alpha(\mathbf{x}) = m_{\text{PDG}}^2 - E^2 + |\mathbf{p}|^2 - \mathbf{H}^{\alpha-1} \cdot (\mathbf{x}^\alpha - \mathbf{x}^{\alpha-1}), \quad (35)$$

with

$$266 \quad \mathbf{H} = \begin{pmatrix} \dots & 2p_x & & & \dots \\ \dots & & 2p_y & & \dots \\ \dots & & & 2p_z & \dots \\ \dots & & & & -2E & \dots \end{pmatrix}. \quad (36)$$

### 3.1.7. Beam spot constraint

268 *B*-mesons have a short lifetime and decay very close the beam spot, therefore it is useful to constrain the reconstructed particles to a volume within that region. The constraint is implemented by considering the initial  $e^+e^-$  collision as an abstract mother particle with the parameters and uncertainties of the beam spot, thus constraining the *production* vertex position of its daughters to an area within the beam spot's three dimensional uncertainty region using

$$274 \quad r^\alpha(\mathbf{x}) = \mathbf{s} - \mathbf{h}_{\text{production}} + \mathbf{H}^{\alpha-1} \cdot (\mathbf{x}^\alpha - \mathbf{x}^{\alpha-1}), \quad (37)$$

with the Jacobian

$$276 \quad \mathbf{H} = \begin{pmatrix} \dots & & \dots \\ \dots & \mathbb{1}_3 & \dots \\ \dots & & \dots \end{pmatrix}. \quad (38)$$

278 Here  $\mathbf{s}$  denotes the beam spot position vector and  $\mathbf{h}_{\text{production}}$  is the fitted production vertex of the particle. The beam spot is determined as part of the detector calibration, by averaging the  $x$ ,  $y$  and  $z$  positions of the  $e^+e^-$  collisions over many interactions. The *decay* vertex can be constrained similarly.

### 3.1.8. Custom Origin constraint

282 Similar to the beam spot constraint, one can construct another geometric  
constraint by defining a custom vertex position and an associated uncertainty  
284 to be the origin of the decay chain. This can be very useful when the decay  
chain contains particles that can not be detected, for example, neutrinos or  
286 long lived dark matter particles. In these decay chains it is not useful to fit the  
full chain, because the missing particle's four momentum makes the kinematic  
288 constraint of the mother particle an incorrect assumption. However, knowing  
that the particle originates from a  $B$ -meson decay, one can define a geometric  
constraint corresponding to the volume where  $B$ -mesons decay on average.  
290

A beam energy constraint is not needed, as one can mass constrain the  $\Upsilon(4S)$   
292 particle, since all four-vectors in  $e^+e^- \rightarrow \Upsilon(4S)$  are well known.

## 4. Fitting complex decay topologies and extracting parameters from the fit

294 In this section we present two use cases of the algorithm containing one and  
two  $\pi^0$ -mesons in a decay chain, respectively. There are numerous channels  
where the phase space is large enough to add  $\pi^0$  to a vertex with two charged  
298 tracks, which makes this a very common structure in decay trees and therefore  
an interesting target to fit in a wide spectrum of analyses. We use Monte Carlo  
300 samples from the Belle II experiment and evaluate background rejection and  
signal resolution improvements, as well as the extraction of various other pa-  
rameters. The selection criteria used for all analyses in this section are listed  
302 in Table 2. We use implicit charge conjugation, meaning that charged parti-  
cles appearing in the decay chains imply including the opposite charges. We  
304 abbreviate decays  $x \rightarrow yz$  as  $x(yz)$ .

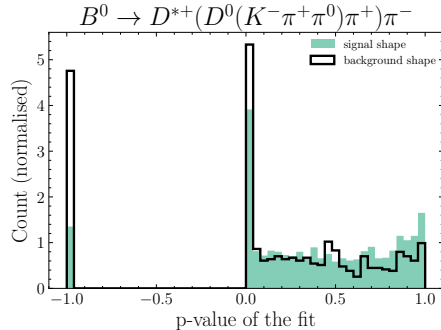
### 4.1. Fitting decay chains containing a neutral particle

306 The first mode, with a single  $\pi^0$ , is  $B^0 \rightarrow D^{*+}(D^0(K^-\pi^+\pi^0)\pi^+)\pi^-$ . This  
channel is of interest as it is the most common  $D^0$  decay modes. We use the  
fitter in this example to suppress background. If we reject combinations for  
308 which the fit failed - i.e. those with a p-value  $\leq 0$  - we are able to reject about  
20% of the background while rejecting only about 4% signal, as displayed in  
310 Fig. 7a. Note that since some of the constraints are nonlinear, the  $\chi^2$  which  
is used to calculate the p-values can be degenerate, where the effective number  
312 of degrees of freedom is smaller than the theoretical one used to calculate the  
p-values. As a result, the p-values can have non-flat shapes [9].  
314

### 4.2. Fitting ill-defined decay vertices

316 We study the decay chain  $B^0 \rightarrow K_S^0(\pi^0(\gamma\gamma)\pi^0(\gamma\gamma))J/\Psi(\mu^+\mu^-)$ . By per-  
forming the fit a large amount of the background can be removed by requiring  
318 that it passes the fit, see Fig. 8a. The only well defined vertex in this chain is  
given by the  $J/\Psi \rightarrow \mu^+\mu^-$  decay. The other vertices are ill-defined, the best  
320 assumption that can be made for the production vertex position of the four





(a)

Figure 7: P-value distributions of fits to  $B^0 \rightarrow D^{*+}(D^0(K^-\pi^+\pi^0)\pi^+)\pi^-$ . The background and signal rejection properties of the p-value are insensitive to the number of DOF. The preselection criteria are listed in Table 2.

322 photons is that they originate from the interaction point. This assumption bi-  
 323 ases the reconstructed mass of the  $K_S^0$ . Performing a fit with mass constrained  
 324  $\pi^0$ -mesons improves the extracted mass of the  $K_S^0$ , so that after the fit, it is  
 325 centred around the true value, as depicted in Fig. 8b. It is then possible to  
 326 further reject background outside the nominal mass window and improve the  
 signal purity when analysing this channel.

#### 328 4.3. Extracting the decay length of $D^0$ -mesons from $D^{*+}$ decays using a beam- 329 spot constraint

330 The geometric constraints allow for the extraction of all the production and  
 331 decay vertices of all particles in the decay chain. This allows for the extraction  
 332 of flight lengths and thus lifetimes of intermediate particles such as  $D^0$ -mesons.  
 333 We perform this study on  $B^0 \rightarrow D^{*+}(D^0(K^-\pi^+)\pi^+)\pi^-$  decays and extract  
 334 the decay length of the  $D^0$ -meson. The results are depicted in Fig. 9. Since  
 335  $D^{*+}$ -mesons decay almost instantly, we will use the three dimensional distance  
 336 between the  $B^0$  and the  $D^0$  decay vertices. To improve the resolution on the  
 $B^0$  vertex we apply a beam-spot constraint.

#### 338 4.4. Using a custom origin constraint to improve the $D^{*+}$ vertex resolution in 339 $B^0 \rightarrow D^{*+}(D^0(K^-\pi^+)\pi^+)l^-\bar{\nu}$ decays

340 In some scenarios one can not fit the entire decay chain e.g. in semi-  
 341 leptonic decays  $B^0 \rightarrow D^*\mu\nu_\mu$ , where the neutrino escapes detection. Since  
 342 the neutrino's four vector is unknown it is not possible to use a kinematic con-  
 343 straint to fit the  $B$ -meson. To circumvent this problem, one can omit fitting  
 344 the  $B^0$ , and instead account for its presence with a geometric constraint. In  
 345  $B^0 \rightarrow D^{*+}(D^0(K^-\pi^+)\pi^+)l^-\bar{\nu}$  decays we use a custom origin constraint to con-  
 346 strain the  $D^{*+}$  production vertices to a volume around the median  $B$ -meson  
 decay vertex position obtained from Monte Carlo simulations. The results are

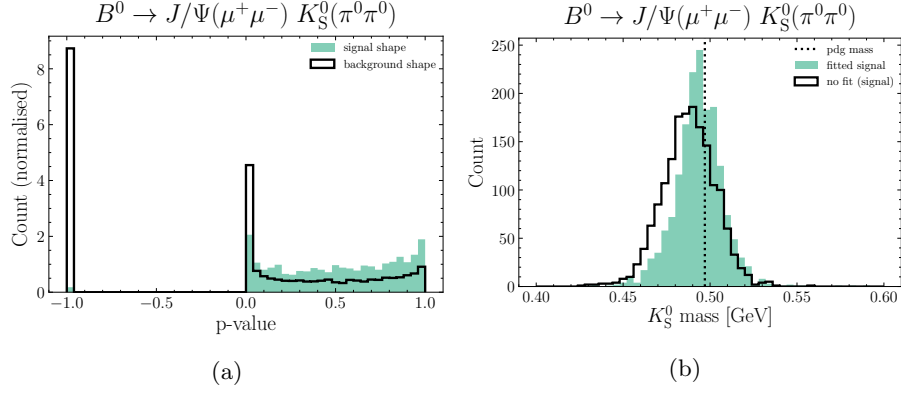


Figure 8: a) P-value of the fits to  $B^0 \rightarrow J/\psi K_S^0$ . b) Fitted mass of the  $K_S^0$  (green) and the mass before the fit (black). The mass distribution is centred around the true value after performing the fits with a  $\pi^0$  mass constraint. The resolution has slightly improved as well.

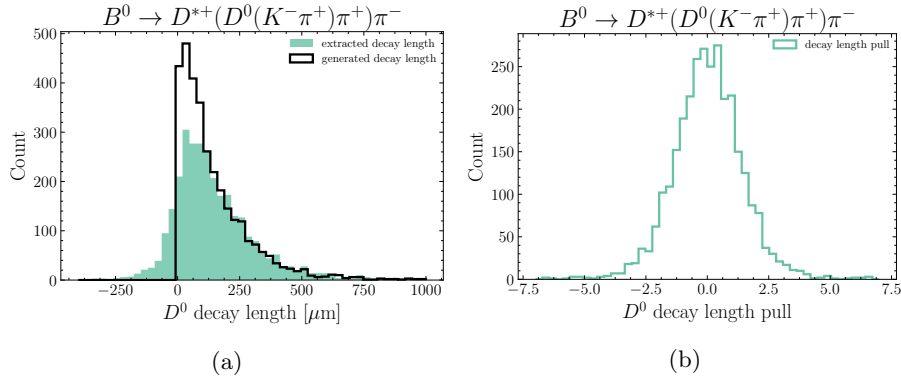


Figure 9: a) The extracted decay length (green) and the generated decay length (black). The negative tail of the extracted decay length is due to the detectors resolution function. b) Pull (measured – generated/uncertainty) of the decay length distribution.

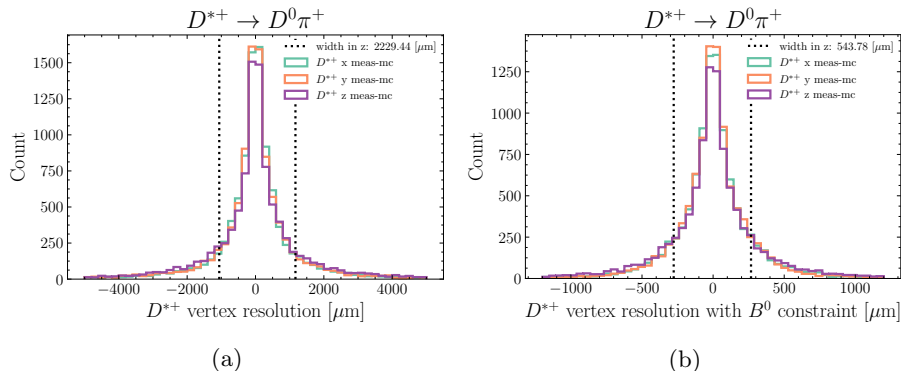


Figure 10: Resolution (= measured - generated) of the  $D^{*+}$  decay vertex position extraction without (a) and with (b) a custom origin constraint. The vertex position and uncertainties for the origin used in this example are extracted from  $B^0$  decays.

Table 2: Selection criteria used in the analyses in this section. All particles use the same criteria if appearing in the decay chains. The invariant mass is obtained by summing the particle's daughter four-momenta before performing the fit. The particle ID for  $K^+/\pi^+$  is defined as the likelihood ratio  $\mathcal{LR}(K^+(\pi^+)) = \mathcal{L}(K^+(\pi^+))/(\mathcal{L}(\pi^+) + \mathcal{L}(K^+))$  and the beam energy constrained mass  $m_{bc}$  [10].

particle	pre selection applied
$\gamma$	$E_\gamma > 0.075$ GeV
$\pi^0$	$0.145$ GeV $> m(\gamma\gamma) > 0.125$ GeV
$\pi^+$	$\mathcal{LR}(\pi^+) > 0.5$
$K^+$	$\mathcal{LR}(K^+) > 0.5$
$D^0$	$1.9$ GeV $> m(K^-\pi^+\pi^0) > 1.7$ GeV
$D^*$	$\Delta m(D^* - D^0) < 0.155$ GeV
$B^0$	$m_{bc} = \sqrt{E_{\text{beam}}^2/4 - p^2} > 5.27$ GeV

348 depicted in Fig. 10. This technique can improve the resolution on the  $D^{*+}$   
349 vertex position.

## 350 5. Conclusion

We presented a versatile fitting tool tailored for the environment of  $B$  factories with a cylindrical detector geometry. It can be used for various purposes, such as the extraction of particle production and decay vertices, decay lengths, particle four-momenta and rejection of backgrounds, as well as the extraction of the respective uncertainties for all parameters involved in three dimensions. This global fitting technique is particularly powerful in fitting and reducing background in modes that contain neutral particles, and will be very important for the Belle II physics analysis program. As a future extension of the fitter we are looking into the possibility to map the residuals found by the Kalman

360 Filter to a scalar signal probability  $f : \mathbf{r} \rightarrow p$ . Such a probability may out-  
perform methods using a p-value derived from the fit  $\chi^2$  for the purpose of  
362 signal-background-separation.

## 6. Acknowledgements

364 This work was made possible by the Belle II collaboration and funding from  
ARC (Australia), ARRS (Slovenia), BMBF (Germany), EXC153 (Germany),  
366 HGF (Germany), INFN (Italy), MSMT (Czech Republic), NSERC (Canada)  
and U.S. DOE. We would like to thank Wouter Hulsbergen for his original  
368 paper, the discussion and sharing his code.

## References

- [1] W. D. Hulsbergen, Decay chain fitting with a Kalman filter, Nucl. Instrum. Meth. A552 (2005) 566–575. [arXiv:physics/0503191](#), [doi:10.1016/j.nima.2005.06.078](#).
- [2] G. Guennebaud, B. Jacob, et al., Eigen v3 (2010).  
URL <http://eigen.tuxfamily.org>
- [3] The Belle II collaboration, Belle ii technical design report [arXiv:1011.0352](#).
- [4] R. E. Kalman, A new approach to linear filtering and prediction problems, Transactions of the ASME–Journal of Basic Engineering 82 (Series D) (1960) 35–45.
- [5] R. Frühwirth, Application of Kalman filtering to track and vertex fitting, Nucl. Instrum. Methods Phys. Res., A 262 (HEPHY-PUB-503) (1987) 444. 19 p.  
URL <https://cds.cern.ch/record/178627>
- [6] C. Patrignani, et al., Review of Particle Physics, Chin. Phys. C40 (10) (2016) 100001. [doi:10.1088/1674-1137/40/10/100001](#).
- [7] V. Karimaki, Effective circle fitting for particle trajectories, Nucl. Instrum. Meth. A305 (1991) 187–191. [doi:10.1016/0168-9002\(91\)90533-V](#).
- [8] N. Dawe. [link].  
URL <https://github.com/ndawe/tikz-track>
- [9] R. Andrae, T. Schulze-Hartung, P. Melchior, Dos and don'ts of reduced chi-squared [arXiv:1012.3754](#).
- [10] E. Kou, et al., The Belle II Physics Book [arXiv:1808.10567](#).